Universality and the thermoelectric transport properties of a double quantum dot system: Seeking for conditions that improve the thermoelectric efficiency

R. S. Cortes-Santamaria[1], J. A. Landazabal-Rodríguez[2], J. Silva-Valencia[1], E. Ramos[3], M. S. Figueira[4] and R. Franco[1⋆].

1 Departamento de Física, Universidad Nacional de Colombia (UNAL), A. A. 5997, Bogotá, Colombia.
2 Departamento de Ciencias Naturales, Escuela Tecnológica Instituto Técnico Central (ETITC), Bogotá, Colombia.
3 Vicerrectoría de Investigaciones, Universidad Manuela Beltrán, Bogotá, Colombia.
4 Instituto de Física-Universidade Federal Fluminense (IF-UFF), Av. Litorânea s/n, CEP:24210-346, Niterói, Rio de Janeiro, Brazil.
⋆ Corresponding author: rfrancop@unal.edu.co

December 23, 2023

Abstract

Employing universal relations for the Onsager coefficients in the linear regime at the symmetric point of the single impurity Anderson model, we calculate the conditions under which the quantum scattering phase shift should satisfy to produce the asymptotic Carnot's limit for the thermoelectric efficiency. We show that a single quantum dot connected by metallic leads at the Kondo regime cannot achieve the best thermoelectric efficiency. We study a serial double quantum dot system, with the quantum dots immersed in ballistic conduction channels. Each QD exhibits a strong but finite local electronic correlation U. We show that maintaining one dot in the electron-hole symmetric point and allowing charge fluctuations in the other QD makes it possible to drive the system to the maximum thermoelectric efficiency.

We also show that the bound states in the continuum (BICs) and quasi-BICs associated with the quantum scattering interference process drive the DQD to the maximum thermoelectric efficiency. We identify two types of quasi-BICs that occur at low and high temperatures: The first is associated with single Fano resonances, and the last is with several Fano processes. We also discussed possible temperature values and conditions that could be linked with the experimental realization of the results.

1   Introduction

The thermoelectric effects in conventional metals have been well-known since the beginning of the 19th century. These effects permit obtaining electricity by employing a temperature gradient (Seebeck effect - thermoelectric generators) or causing a temperature gradient using an electrical potential difference (Peltier effect - thermoelectric refrigerators). Unfortunately, in conventional metals, the thermal efficiency associated with these effects is very low due to the interdependent character of the electrical and thermal conductances. These effects allow the development of thermoelectric generators (TEGs) that only acquire some practical applications after the discovery that the doped semiconductor Bi_2Te_3 and its alloys Sb_2Te_3, and Bi_2Se_3 [1–3], present at room temperatures a higher dimensionless thermoelectric figure of merit (ZT) [1,4] and a high power factor (PF) and, until now, dominate the commercial industry of TEGs [5].

Due to environmental pollution problems, TEGs have recently started to be used as a thermoelectric energy recovery to convert wasted heat into electric power. Two promising applications where the TEGs have been used are automotive energy recovery and hybrid solar energy converter systems. In the first case, the TEG is generally coupled to the exhaust gas system once the primary waste energy flows from this vehicle device. Gasoline vehicles present a better power output than diesel vehicles, and this energy could be used to power the car's electrical devices and improve engine performance [6]. In the second application, photovoltaic cells, only the photons with energies close to the cell band gap contribute to an effective electric conversion. The energy of the photons greater than the cell band gap is dissipated as heat. A hybrid solution involves attaching a TEG to the back of the cell to convert the wasted heat into electric power. Some experimental results show that the electric efficiency of the PV-TE system should be enhanced at around 8% when compared with the PV solar system alone [6].

Since the experimental realization of the single impurity Anderson model (SIAM) employing a quantum dot immersed into a two-dimensional electron gas (single electron transistor - SET) [7], the interest in the research on nanostructured devices has been growing continuously. The thermoelectric properties of a quantum dot (QD) in the presence of Kondo correlations were addressed in an experimental device in references [8,9]. The employment of nanoscopic systems as thermal rectifiers shows that it is possible to enhance the efficiency of macroscopic devices by controlling energy transport on a microscopic scale [10]. A recent experiment measured the thermoelectric properties in the Kondo limit of a correlated QDs device [11], below and above the Kondo temperature, producing high-quality data that allows a quantitative comparison with numerical renormalization group (NRG) results [12]. Another recent experiment [13] realizes a thermoelectric conversion at temperatures around $T = 30K$ in $InAs/InP$ nanowire QDs by taking advantage of their strong electronic confinement. We

can cite the following papers from the theoretical perspective [14–26] and others from the experimental point of view [11, 13, 27–31]. Furthermore, recent reviews can provide enriching insights into the topic [32–34].

In the theoretical calculations of this work, we neglect the phonon lattice contribution to thermal conductance. However, this approximation is perfectly justifiable due to the high degree of phonon emission process control attained recently by experimental realizations of the DQD geometry [35, 36]. In reference, [35], the authors have measured phonon emission rates in a GaAs/AlGaAs DQD; the isolation of the system from electronic reservoirs, the low temperatures, and the weak tunnel coupling compared to values of detuning allowed for a direct readout of the interaction spectral density of electron-phonon coupling. On the other hand, in reference, [36], the authors studied a serial DQD formed in an $InAs/InP$ nanowire coupled to two electron reservoirs. They obtained phonon-assisted transport, allowing the conversion of local heat into electrical power in a nanosized heat engine.

Bound states in the continuum (BICs) are generally valid for waves, including the wave functions of quantum mechanics. BICs remain localized even though they coexist with a continuum spectrum of waves that could dissipate energy [37]. Although this phenomenon was proposed in the context of quantum mechanics [38], it appears in many different classical and quantum systems [37, 39, 40]. BICs are localized states in the continuum spectrum with discrete energies or frequencies, invisible to manipulation once the transmittance does not exhibit its presence [41, 42].

On the other hand, Fano resonances appear when there is a quantum interference process in a system consisting of a continuous degenerated spectrum connected to a system that exhibits a discrete level spectrum [43]. The interference is produced among the electrons circulating along the system's two channels: the discrete levels and the continuous conduction bands. Generally, by detuning the system from the BIC conditions, for example, changing the hybridization between the leads and the dots, the BICs transform themselves to Fano resonances (quasi-BICs) [44, 45] exhibiting dips in the transmission spectra and sharp peaks in the density of states (DOS).

Theoretical calculations and DFT simulations [46–49] predict that Fano resonances formed crossing or near the chemical potential contribute to the increase of the ZT parameter. This condition is only a realization of the Mahan-Sofo criteria [50] that predicts the best ZT for the presence of a delta function in the density of states near the chemical potential. The reference [51] presents a critical discussion about this point. One example of this kind of system is the use of porphyrin-based molecules with different metal centers, like the family of metals Mn, Co, Ni, Cu, Fe, and Zn, connected to gold electrodes to form a single electron transistor (SET) [52–55].

The main result of this paper is to show that the optimal values of the phase shifts generated by the quantum scattering interference process in a double quantum dot system (DQD) produce maximum thermoelectric efficiency. When tuned by an external parameter like the hybridization or temperature, these phase shifts generate quasi-BICs in the density of states, which are responsible for the considerable increase of the dimensionless thermoelectric figure of merit ZT.

In Sec. 2, we define the model and the computation of the thermoelectric transport coefficients. In Sec. 3, we express the ZT product in terms of the Mahan-Sofo parameter ε, employing the universal relations obtained in a previous paper [56]. Furthermore, we explore the quantum scattering process of getting the Carnot's machine limit for a single SET ($ZT \rightarrow \infty$, $\varepsilon \rightarrow 1$). In Sec. 4, we describe a system of DQDs, showing two conditions that create an effective quantum scattering phase shift that significantly improves the thermoelectric efficiency. In section 5, we present the discussion of the role of quasi-BICs linked to the enhancing process of ZT at low temperatures. In section 6, we discuss the best conditions to

obtain the enhancement of ZT at high temperatures and the quasi-BICs generated by thermal excitations associated with rising multiple Fano resonances. Section 7 presents the conclusions and perspectives of this paper. Appendix A summarizes the cumulant Green's functions method employed in all the thermoelectric calculation properties. Appendix B contains a derivation of the thermoelectric transport properties and a short discussion of the efficiency power.

2   Model and Theory
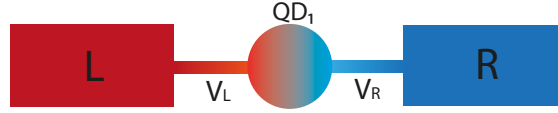
Figure 1: (Color online) Schematic picture of a quantum dot embedded into conduction leads (single electron transistor - SET).

Fig. 1 presents a pictorial view of the single electron transistor. The Hamiltonian of the system can be written as

$$
H = \sum_{\mathbf{k},\sigma} \sum_{\alpha=L,R} E_{\mathbf{k},\sigma}^{\alpha} c_{\mathbf{k},\sigma}^{\alpha\dagger} c_{\mathbf{k},\sigma}^{\alpha} + \left(E_d n_d + U n_{d\uparrow} n_{d\downarrow} \right)
$$
$$
+ \sum_{\alpha=L,R} \sum_{\mathbf{k},\sigma} \frac{V_\alpha}{\sqrt{2N}} \left(c_{d\sigma}^{\dagger} c_{\mathbf{k},\sigma}^{\alpha} + c_{\mathbf{k},\sigma}^{\alpha\dagger} c_{d\sigma} \right), \tag{1}
$$

where the first term represents the conduction leads, characterized by free conduction electrons (c-electrons) to the right (R) and the left (L) of the QD (Fig. 1), the second term describes the QD, where U represents the Coulomb repulsion between the electrons at the QD site and the dot energy E_d, controlled by the gate voltage [57,58], and the third term corresponds to the tunneling between the embedded dot and the left (L) and right (R) semi-infinite leads. The amplitude V_α is responsible for the tunneling between the QD and the lead α. For simplicity, we assume symmetric junctions (i.e. $V_\alpha = V_L = V_R = V$) and identical leads (i.e., $E_{\mathbf{k},\sigma}^{L} = E_{\mathbf{k},\sigma}^{R} = E_{\mathbf{k},\sigma}$) connecting the QD to the quantum wire, which will be described by a structureless rectangular conduction band of width, $W = 2D$.

All the calculations are made using the cumulant Green's function method (CGFM) for the SIAM described in Appendix A [59], considering that Friedel's sum rule is satisfied numerically with an error percentage under the 1%. The method can be summarized as follows: 1. Diagonalize a Wilson chain composed of N sites, here $N = 2$, with one impurity site and one conduction site. 2. Employing the Lehmann representation to calculate all the allowed atomic cumulant Green's functions (GFs). 3. Collect all the atomic GFs with non-zero residues and use them to calculate the atomic cumulants. 4. These atomic cumulants are approximations to calculate the full SIAM GFs.

3   Thermoelectric figure of merit and universality

In Appendix B, we derive the transport coefficients $L_0(T)$, $L_1(T)$, and $L_2(T)$, and the thermoelectric properties. In this section, we study the enhancement of the thermal efficiency of the SET, depicted in Fig. 1 and described by the Hamiltonian of Eq. 1, to produce the asymptotic Carnot's limit for the thermoelectric efficiency. We employed universal relations obtained as a function of the temperature normalized by the Kondo temperature $T^* = \frac{T}{T_K}$, and valid for the

SIAM in the Kondo regime [56]. We investigated the dimensionless thermoelectric figure of merit ZT [60] as a function of T^*, associated with the thermoelectric efficiency as a function of the Mahan-Sofo parameter ε [50]. The ZT is defined by

$$ZT = \frac{S^2 T G}{K + K_{ph}}, \tag{2}$$

where G is the electrical conductance, S is the thermoelectric power, T is the absolute temperature [Eqs. (37), (40) and (41)]. K_{ph} is the contribution of the phonons to thermal conductance that tends to decrease ZT; however, for simplicity, we do not consider the K_{ph} contribution in this paper. A recent critical discussion of the evolution of the best thermoelectric efficiency can be found in the reference [61].

Following the work of G.D. Mahan and J. O. Sofo [50], we define the Mahan-Sofo parameter ε as a function of the thermoelectric coefficients, derived in Appendix B,

$$\varepsilon = \frac{L_1^2(T)}{L_o(T) L_2(T)}. \tag{3}$$

The Mahan-Sofo parameter ε depends only on the thermoelectric coefficients, and it can be calculated employing the Boltzmann equation, the Landauer formalism, or any other pertinent method. In the original paper of Mahan and Sofo, they employed the Boltzmann formalism and used the transport distribution $\Sigma(\epsilon)$. In the present paper, we are interested in studying BICs resulting from the system's quantum interference processes. For this reason, we use the Landauer formalism and calculate the electronic transmittance, $\mathcal{T}(\omega)$. On the other hand, those two quantities only agree within the semiclassical Boltzmann limit. The inclusion of the electronic correlation that justifies the presence of the Kondo effect in the single electron transistor (SET) was derived in reference [62]. The QD was described by the Anderson impurity model, connected to the leads at different temperatures, within the Keldysh nonequilibrium Green's function formalism. The transport coefficients L_n,Eq. 42, were calculated, considering the particle current and thermal flux formulas through an interacting QD, [14–19]. In the present paper, the correlation in the system is "incorporated" into the electronic transmittance and computed by the CGFM, described in Appendix A.

Employing Eqs. (37), (40) and (41), the dimensionless thermoelectric figure of merit, defined from Eq. (2), can be written as

$$ZT = \frac{\varepsilon}{1 - \varepsilon}. \tag{4}$$

It is clear from the above equation that the best dimensionless thermoelectric figure of merit ZT occurs at the limit $\varepsilon \to 1$. In a previous paper [56], we showed that in the Kondo regime, the following equations are valid:

$$L_0(T^*) = -\left(L_0^S(T^*) - \frac{1}{h} \right) cos(2\delta) + \frac{1}{h}, \tag{5}$$

$$\frac{L_1(T^*)}{T^*} = \frac{L_{01}^S(T^*)}{T^*} sin(\delta) cos(\delta), \tag{6}$$

and

$$\frac{h L_2(T^*)}{(k_B T^*)^2} = -\left(\frac{h L_2^S(T^*)}{(k_B T^*)^2} - \frac{\pi^2}{6} \right) cos(2\delta) + \frac{\pi^2}{6}, \tag{7}$$

with $T^* = \frac{T}{T_K}$, being the temperature "normalized" by the Kondo temperature T_K, $L_0^S(T^*)$ is the coefficient $L_0(T^*)$ computed in the symmetric point of the model; an analogous situation

exists for $\frac{hL_2^S(T^*)}{(k_BT^*)^2}$. These two functions, together with $\frac{L_{01}^S(T^*)}{T^*}$ are universal functions of T^* and were computed employing NRG in a previous paper [56]. The parameter δ is the quantum phase shift associated with the Kondo scattering and "carries" the dependence with all the other parameters of the system.

Employing Eqs. 5, 6 and 7 in Eq. 3 we obtain

$$\varepsilon(T^*) = \frac{L_1^2(T^*)}{L_o(T^*)L_2(T^*)} = \sin^2(2\delta)\big[A(T^*)\cos^2(2\delta) + $$
$$B(T^*)\cos(2\delta) + C(T^*)\big]^{-1}, \tag{8}$$

where $A(T^*)$, $B(T^*)$ and $C(T^*)$ are universal expressions of T^* given by:

$$A(T^*) = \frac{4\big[L_0^S(T^*) - \frac{1}{h}\big]}{L_{01}^2(T^*)} \times \left[\frac{hL_2^S(T^*)}{(k_BT^*)^2} - \frac{\pi^2}{6}\right](k_BT^*)^2, \tag{9}$$

$$B(T^*) = \frac{-4(k_BT^*)^2}{L_{01}^2(T^*)} \times \left[\left(L_o^S(T^*) - \frac{2}{h}\right)\frac{\pi^2}{6} + \frac{\frac{1}{h}L_2^S(T^*)}{(k_BT^*)^2}\right], \tag{10}$$

and

$$C(T^*) = \left(\frac{2\pi^2}{3h}\right)\frac{(k_BT^*)^2}{L_{01}^2(T^*)}. \tag{11}$$

Using $sin^2(2\delta) = 1 - cos^2(2\delta)$ in Eq. 8, and considering $\varepsilon(T^*) = 1$ we obtain a quadratic equation for $cos(2\delta)$

$$\cos^2(2\delta)(A(T^*)+1) + B(T^*)\cos(2\delta) + C(T^*) - 1 = 0. \tag{12}$$

To obtain the best thermal efficiency of the system on a temperature (T^*), we must achieve $\varepsilon(T^*) = 1$, which means solving the equation in terms of the scattering phase shift,

$$\cos(2\delta) = \frac{-B(T^*) \pm D(T^*)}{2[A(T^*)+1]}, \tag{13}$$

where $D(T^*)$ is a universal function of (T^*) given by

$$D(T^*) = \sqrt{B^2(T^*) - 4[A(T^*)+1][C(T^*)-1]}. \tag{14}$$

Next, we calculate the limits of low and high temperatures of Eqs. 5, 6 and 7, analytically. Using these results, we show that in the first case exist two solutions for Eq. 13 associated with $\delta = \pi/4$ or $\delta = 3\pi/4$, at intermediate temperatures when the C=1, and in the limit of high temperatures exist only one solution with $\delta = \pi/2$. The universal functions in the limit of low temperatures $T^* \to 0$ have the following values: $L_0^S = 1$, $\frac{L_{01}^S}{T^*} = 0$, and $\frac{hL_2^S(T^*)}{(k_BT^*)^2} = \pi^2/3$. At high temperatures, in the limit when $T \to \infty$: $L_0^S = 0$, $\frac{L_{01}^S}{T^*} = 0$, and $\frac{L_2^S(T^*)}{(k_BT^*)^2} = 0$ [56].

Eq. 13 is valid in the Kondo regime, where the expected quantum phase scattering is $\delta \simeq \pi/2$ at low temperatures $T^* < 1$. However, in this regime, we found the two solutions ($\delta = \pi/4$ and $\delta = 3\pi/4$), as indicated in Fig. 2, that do not satisfy the Friedel sum rule, [59], and imply that is impossible to achieve the best thermoelectric efficiency for the SET.

In Fig. 2, we plot the two "branches", corresponding to the (+) and (−) solutions, for the right side of Eq. 13. The dotted horizontal lines are associated with possible solutions for the δ parameter. The dotted line in 1.0 is associated with a value of $cos(2\delta) \simeq 1$, which presents a unique solution at $\delta \simeq 0.0$, that is a trivial solution and corresponds to having a ballistic channel in all the temperature ranges. When the "branch" associated with the root (−) is crossed by the dotted line at zero, at the red dot, two possible solutions are defined:
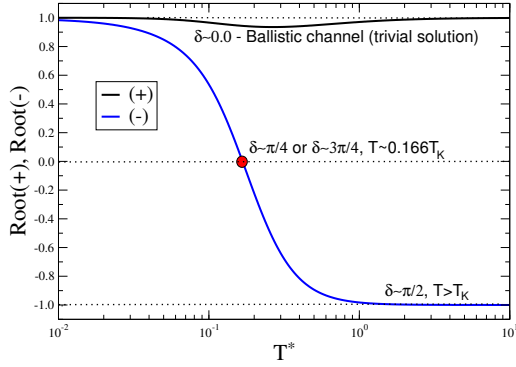
Figure 2: (Color online) Two possible "branches" of the right side of Eq. 13 vs. ($T^* = T/T_K$). The dotted lines show the solutions of Eq. 13.
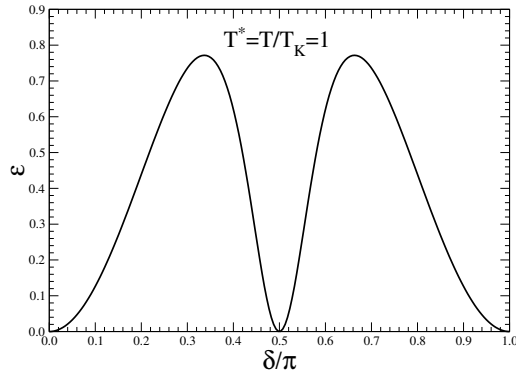
Figure 3: (Color online) The ε parameter as a function of the quantum phase scattering δ/π, for $T^* \simeq 1$.

$\delta \simeq \frac{\pi}{4}$ and $\delta \simeq \frac{3\pi}{4}$ at $T \sim 0.166 T_K$. For the bottom dotted line in -1.0, it is possible to obtain a unique solution $cos(2\delta) \simeq -1$, $\delta \simeq \frac{\pi}{2}$ for high temperatures $T^* > 1$.

Fig. 3 shows an estimation of the Mahan-Sofo parameter ε as a function of δ/π, for $T^* \simeq 1$. The ε was computed employing the universal values for Onsager's coefficients, Eqs. 9-11, as a function of T^* obtained in reference [56] and the Eq. 8. At around the values $\delta \simeq 0.33\pi \simeq \pi/4$ and $\delta \simeq 0.66\pi \simeq 3\pi/4$, values of $\varepsilon \simeq 0.8$ are obtained, which corresponds to a $ZT \simeq 4$. For $\delta = \pi/2$, $\varepsilon = 0$ corresponds to the model's symmetric point, where the Kondo resonance is present, and the thermopower vanishes [63].

The impossibility of attaining Carnot's efficiency for a SET in the Kondo regime in those systems does not invalidate the research of SETs as QD heat engines. One example of this is a recent work of a SET out of the equilibrium regime [64] that exhibits an efficiency in excess of 70% of the Carnot's efficiency while maintaining a finite power output. The experiment was performed in an out-of-equilibrium condition. However, the higher temperature difference between the hot (T_h) and the cold (T_c) reservoirs is given by $\Delta T = T_h - T_c \simeq 0.7K \simeq 7.0 \times 10^{-2}\Delta$, which is a small value that justifies the comparison with the results exposed in Fig. 3, obtained in the linear regime. Here, we employ an estimative of our energy unit $\Delta \sim 10K$ obtained by comparison of our theoretical results for electrical conductance at the unitary limit with experimental ones [63]. This experimental result [64] is in qualitative agreement with recent theoretical papers [65–67] that compute thermoelectric properties for a single QD system out of the equilibrium. They reported high thermoelectric performances when the QD has a single occupation, showing that the thermopower exhibits a change of sign due to the Kondo correlations at non-equilibrium conditions originated by asymmetrically tunneling to exter-

nal electrodes. Those results are also compatible with the fact that the single SET does not exhibit Fano resonances near the chemical potential that could contribute to increases ZT values. However, another promising system that could have its thermal efficiency increased is the metalloporphyrins QDs connected to gold leads, [47, 52, 54]. These systems exhibit Fano resonances near the chemical potential due to quantum interference processes from the symmetry-dependent coupling between molecular orbitals.

4 Two coupled identical quantum dots: Seeking for conditions that improve the thermoelectric efficiency

This section describes a system of two identical QDs (QD1 and QD2), a DQD system, as represented schematically in Fig. 4. Each QD exhibits a strong but finite local electronic correlation U. The QDs are connected by a conduction band (CB) through hybridizations V_{QD1} and V_{QD2} and immersed in a ballistic conduction channel. We consider the two QDs sufficiently separated to neglect their inter-dot correlations so that the SIAM could describe each one, and their interaction occurs via the conduction band CB. The Hamiltonian of the DQD reduces to two Hamiltonians of the one QD as presented in Eq. 1 of the paper. It happens because there is no kind of hybridization connecting the two QDs.
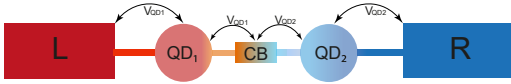
Figure 4: (Color online) Schematic picture of the DQD setup composed of two serial quantum dots, QD_1 and QD_2 immersed into conduction bands L, CB, and R, and subjected to the hybridizations V_{QD1} and V_{QD2}.

In this section, we calculate an effective quantum phase shift δ_{eff} that could improve the thermoelectric efficiency and allow achieving the asymptotic Carnot's limit associated with the best thermoelectric efficiency. The $QD2$ is put in the electron-hole symmetry, while the gate voltage E_d is varied in the $QD1$. The correlation in the localized states and the quantum scattering processes originated by the different regimes of the two dots causes an δ_{eff} analogous to the quantum scattering required to improve ZT, and it would be possible to enhance the thermoelectric efficiency.

Eq. 13 was obtained in the Kondo regime at low temperature and around the SIAM's symmetric point, which satisfies the particle-hole symmetry. The spin-flip scattering processes originate the Kondo peak in the density of states, which starts to "disappear" above the Kondo temperature due to thermal fluctuations. However, we can use Eq. 13 to approximate temperatures of the order of the Δ energy scale.

In the DQD setup, the transmission employed to compute the Onsager linear coefficients of Eq. (42) is given by [68]

$$\mathcal{T}(\omega) = \Gamma^2 |G_{00}^{\sigma}(\omega)|^2, \tag{15}$$

where $\Gamma = \frac{V_2^2}{\Delta}$, $\Delta = \frac{\pi V_{QD2}^2}{2D} = 0.01$ is the Anderson parameter that defines the energy unit employed in all the calculations; and $D = 100\Delta = 1$ is the halfwidth of the conduction band. The local dressed Green's function is obtained from the setup of the DQD depicted in Fig. 4

and is given by

$$
\begin{aligned}
G_{00}^{\sigma}(\omega) &= \left[G_c^{\sigma}(\omega) \right]^3 V_{QD1}^2 G_{QD1}^{\sigma}(\omega) V_{QD2}^2 G_{QD2}^{\sigma}(\omega) \\
&= \left[G_{cond}^{\sigma}(\omega) \right]^2 V_{QD2}^2 G_{QD2}^{\sigma}(\omega) \\
&= i Im\left(G_{00}^{\sigma}(\omega) \right) + Re\left(G_{00}^{\sigma}(\omega) \right) \\
&= \left| G_{00}^{\sigma}(\omega) \right| e^{i\delta_{00}(\omega)},
\end{aligned}
\tag{16}
$$

where $G_{QD1}^{\sigma}(\omega)$ and $G_{QD2}^{\sigma}(\omega)$ are the correlated Green's functions associated with the first and second QD, respectively. These Green's functions are calculated through the CGFM, as presented in the appendix A. $G_c^{\sigma}(\omega)$ is the Green's function of the ballistic conduction channels, represented in the Fig. 4 by the labels "L", "CB" and "R", respectively. For simplicity, we use, in all the calculations, an uncorrelated rectangular conduction band of bandwidth $2D$

$$
\rho_c^{\sigma}(E_{\mathbf{k}\sigma}) = \left\{ \begin{array}{ll} \frac{1}{2D} \, , & \text{for } -D \le E_{\mathbf{k}\sigma} - \mu \le D \\ 0 & \text{, otherwise} \end{array} \right. ,
\tag{17}
$$

with the corresponding GF

$$
G_c^{\sigma}(\omega) = \frac{1}{2D} \ln\left(\frac{\omega + D + \mu}{\omega - D + \mu} \right).
\tag{18}
$$

The phase shift associated with the local GF is

$$
\delta_{00}(\omega) = 2\delta_{cond}(\omega) + \delta_{QD2}(\omega),
\tag{19}
$$

$\delta_{cond}(\omega)$ is the phase shift associated with the "effective conduction channel" given by Eq. 21, and $\delta_{QD2}(\omega)$ is the QD2 phase shift set in the Kondo regime. These two path quantum interference processes can produce BICs and quasi-BICs (Figs. 6 and 11). The DQD system studied here behaves analogously to the geometrical configuration of a QD side coupled to a ballistic quantum wire (QW). Where it is clear the presence of a Fano resonance, characterized by the quantum interference of a "resonant" quantum scattering channel (the QD) and the "effective conduction channel" given by Eq. 21. The local phase shift associated with the quantum scattering process in the system can also be written as

$$
\delta_{00}(\omega) = tan^{-1}\left(\frac{Im(G_{00}^{\sigma}(\omega))}{Re(G_{00}^{\sigma}(\omega))} \right).
\tag{20}
$$

The local "effective conduction channel" is described by the Green's function

$$
G_{cond}^{\sigma}(\omega) = \left[(G_c^{\sigma}(\omega))^3 V_{QD1}^2 G_{QD1}^{\sigma}(\omega) \right]^{\frac{1}{2}}.
\tag{21}
$$

The DQD system can be seen as a single QD (QD2) "tuned" in the symmetric point and immersed in a conduction channel, with the leads renormalized given by Eq. 21. We can describe the DQD using the same Hamiltonian of the single QD of section 2, but using the local "effective conduction channel" given by Eq. 21. The average local quantum phase shift ("effective delta parameter", δ_{00}) depends on the thermal fluctuations and the charge fluctuations on the first QD and can be written as

$$
< \delta_{00} > = \int_{-D}^{D} \left(-\frac{\partial f(\omega, T)}{\partial \omega} \right) \delta_{00}(\omega) d\omega,
\tag{22}
$$

where, in all the calculations, Eq. 22 is used to calculate the averaged phase shifts. In particular, we refer to $\delta_{eff} = < \delta_{00} >$. The other two phase shifts will be referred as $\delta_{cond} = < \delta_{cond} >$ and $\delta_{QD2} = < \delta_{QD2} >$.

In the two next sections, we will explore, at low and intermediate temperatures, possible solutions of Eq. 13 for $\delta_{eff} \simeq \frac{\pi}{4}$ and $\delta_{eff} \simeq \frac{3\pi}{4}$. For temperatures above the Δ scale, with solutions at $\delta_{eff} \simeq \frac{\pi}{2}$, we will consider that Eq. 13 is approximately valid. We set the QD2 at the symmetric point of the SIAM as a scattered center and search for a quantum scattering interference process associated with charge fluctuations in the QD1, as pointed out in Eq. 19. In that case, it could originate an effective phase shift that improves thermoelectric efficiency, including the most interesting solution $cos(2\delta_{eff}) \simeq -1$, $\delta_{eff} \simeq \frac{\pi}{2}$ for temperatures above the temperature Δ scale. It is possible to obtain high ZT values if $0 < \delta_{eff} \leq \frac{\pi}{2}$, with the solution at $\delta_{eff} \sim \frac{\pi}{4}$; or if $\frac{\pi}{2} \leq \delta_{eff} < \pi$, with the solution $\delta_{eff} \sim \frac{3\pi}{4}$.

5 Quasi−BICs linked to the enhancing process of ZT: Low temperature regime

The geometrical configuration of the QDs used in this paper is similar to the one employed in reference [69], where the authors considered two square cavities (two-dimensional quantum dots without any electronic correlation), serially connected by an infinite quasi-one-dimensional wire, where electrons have a continuous spectrum of energy. The appearance of BICs is controlled by the variation of the parameters associated with the QDs, their energy levels, and their spatial separation at zero temperature. Another interesting DQD system connected to a finite Majorana Kitaev chain was studied in reference [70], where the authors propose this system to encrypt Majorana fermions qubits as BIC states.

The system in the present paper is also composed of two QDs, serially connected by uncorrelated conduction bands, where electrons also have a continuous spectrum of energy given by Eq. 18. All the three conduction bands represented in the setup of Fig. 4 are ballistic leads and the scattering on the QDs are coherent resulting only in phase shifts of the electronic wave functions that are identified by the Friedel phase shift [71]. Buttiker et al. [72, 73], showed that it is not correct to identify the Friedel phase with the phase of the amplitude of transmission because the transmission phase can depart from the Friedel phase and exhibit a nonanalytic behavior at points where the modulus of the transmission vanishes, while the Friedel phase remains continuous as a function of the energy. However, Orellana [74] showed that the Friedel phase in the presence of BICs is discontinuous as a function of the energy due to the delta-shaped character of the density of states as represented in Fig. 6(a,e).

To check the appearance of BICs in the DQD setup, we introduce an asymmetry in the hybridization at low temperatures, maintain fixed the hybridization V_{QD2}, and vary V_{QD1}. The interference process associated with the BICs is generally a single-particle interference effect. However, this effect can also appear in setups where the QDs exhibit electronic correlation effects U_{12}, as in the DQD geometry studied in reference [75], where the formation of BICs results from a quantum interference process that can be driven by the cross-correlation effects between the two QDs, U_{12}, and the asymmetries in dot-lead couplings. In the DQD studied in this paper, the electronic correlation, as well as the hybridization between the QDs, can act as driven parameters that generate Fano resonances at low temperatures, as plotted in Fig. 6, and multiple Fano resonances at higher temperatures, as exhibited in Fig. 11.

The unit of energy employed in the calculations is the Anderson parameter $\Delta = \frac{\pi V_{QD2}^2}{2D} = 0.01$, with $D = 100.0\Delta$, as defined below Eq. 15, which also furnishes the reference hybridization $V_0 = \sqrt{\frac{2D}{\pi}} = 0.798D$. We estimated the order of magnitude of Δ, using experimental results of the electrical conductance G at low temperatures. At the unitary limit in the Kondo regime for $GaAs(Al)$ [76] and $InAs(InP)$ [77] nanosystems, obtaining $\Delta \simeq 10K \simeq 10^{-3}eV$. At low temperatures, we fix the calculations at the temperature value $T = 0.01\Delta \simeq 0.1K$ because
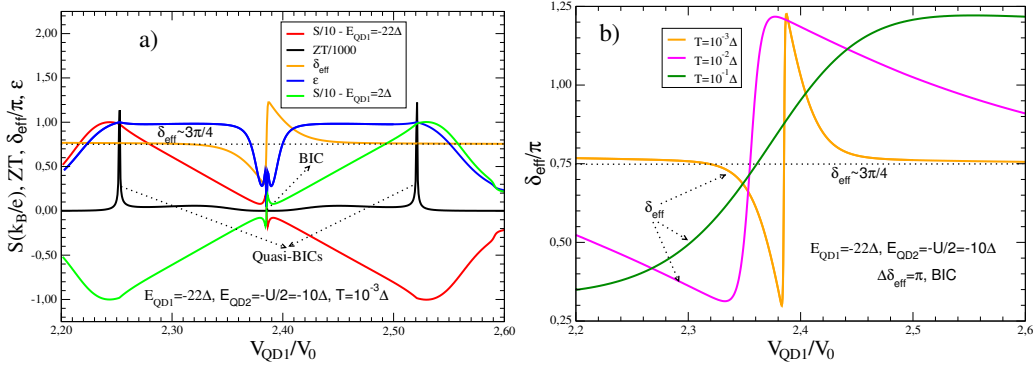
Figure 5: (Color online) Representative values of the QD1 hybridization to obtain quasi-BICs that manifest as strong peaks in the ZT. b) Detail of the δ_{eff} for different temperatures.

this temperature is sufficiently low for the system to show the presence of the Kondo effect. The remaining parameters for the QDs are the electronic repulsion $U_1 = U_2 = 20\Delta$, and the chemical potential $\mu = 0$. We fixed the localized energy levels of the QD2 in the particle-hole symmetric condition, $E_{QD2} = -\frac{U_2}{2} = -10\Delta$, whereas the localized level of the first QD, E_{QD1} is allowed to vary.

In Fig. 5(a,b), we plot the representative values of the QD1 hybridization used in Fig. 6 to obtain quasi-BICs. In Fig. 5a) we calculate the thermopower S for the two conditions with $E_{QD1} = -22.0\Delta$ and $E_{QD1} = 2.0\Delta$, that exhibit an anti-symmetrical shape as indicated by the red and green curves. The maximum ZT values are attained for two hybridizations: $V_{QD1} = 2.25V_0$ and $V_{QD1} = 2.52V_0$; ZT present huge peaks resulting from a quasi-BIC formation near $\mu = 0$, at $(\omega - \mu) \simeq \pm 10^{-2}\Delta$ (see Fig. 6(a,e)), which originates high values of the ε parameter. The symmetrical condition, where $S = 0$, is attained when $V_{QD1}/V_0 = 2.38$ (the mean point between the two ZT maxima). In Fig. 5b) δ_{eff} exhibits a "jump-discontinuity variation" of $\Delta(\delta_{eff}) \simeq \pi$ at the lowest temperature ($T = 10^{-3}\Delta$), evidencing the presence of a BIC in this point [73, 74, 78]. However, δ_{eff} is "smoothed" as the temperature increases. We also should stress that the same parameter set of Fig. 5(a, b), but with $E_{QD1} = 2.0\Delta$ produces similar results, but with $\delta_{eff} \simeq \pi/4$.
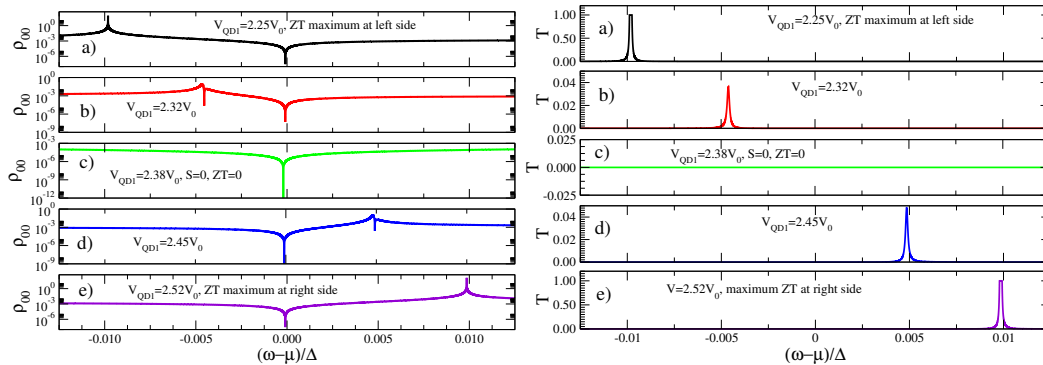
Figure 6: (Color online) Local density of states $\rho_{00}(\omega)$ and the transmittance $\mathcal{T}(\omega)$ vs. ω for representative values of V_{QD1}/V_0 as indicated in Fig. 5(a).

In Figs. 6 (a, b, c, d, e), we plot the local density of states $\rho_{00}(\omega)$ and the transmission coefficient $\mathcal{T}(\omega)$ vs. ω for different values of V_{QD1}/V_0, with $T = 0.01\Delta$ and $E_{QD1} = -22.0\Delta$. This figure shows the emergence of a single BIC, for $V_{QD1} = 2.38V_0$ (Figs. 6(c)), and two quasi-BICs for $V_{QD1} = 2.25V_0$ and $V_{QD1} = 2.52V_0$ (Figs. 6(a,e)), originating from the interaction of

charge fluctuations in QD1 and the Kondo effect in QD2. For the $V_{QD1}/V_0 = 2.38$, the density of states $\rho_{00}(\omega)$ presents a sharp minimum close to $\omega = 0$ and the transmittance $\mathcal{T}(\omega) = 0$. On the other hand, varying the hybridization V_{QD1}/V_0 from this point to the maximum $\mathcal{T}(\omega)$ represented in graphs a) and e) the quasi-BICs emerge and reach their maximum intensities, producing enormous values of ZTs, as indicated in Fig. 5a).
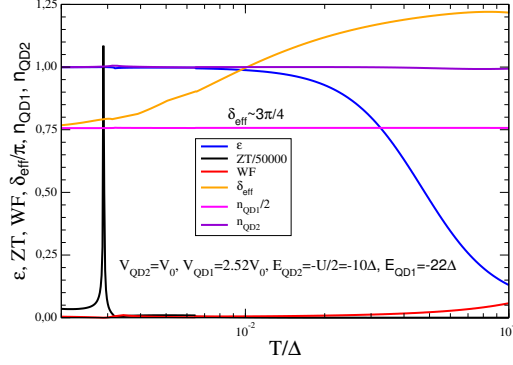
Figure 7: (Color online) The ε parameter and related quantities, at low temperatures, for $V_{QD1} = 2.52V_0$.

Fig. 7 present thermoelectric properties computed for $V_{QD1} = 2.52V_0$, at low temperatures, when $E_{QD1} = -22.0\Delta$; ε is close to the unit, $\varepsilon \simeq 1.0$, and achieves an efficiency at finite output power, Eq. 44, $\eta_{fo} \simeq \eta_C$, close to the Carnot efficiency η_C, for a large range of temperatures below $T \leq 4 \times 10^{-2}\Delta$. The $\delta_{eff} \simeq 3\pi/4$ and the Wiedemann-Franz parameter (WF) is very low (no Wiedemann-Franz behavior (NWF))($WF = \frac{\kappa}{GL_N T} = \frac{3e^2\kappa}{TG\pi^2 k_B^2}$, L_N is the Lorenz's number and k_B is the Boltzmann's constant). This figure reveals that the Kondo effect present in the QD2 ($n_{QD2} \simeq 1$) is an important element that originates the conformation of the quantum-interference scattering process that enhances ZT in a low-temperature range of approximately one order of magnitude. A similar result was obtained for the same parameters when $E_{QD1} = 2.0\Delta$; in this case, $\delta_{eff} \simeq \pi/4$, and the thermopower has a negative sign, indicating a hole thermal conduction processes.

6 Quasi−BICs linked to the enhancing process of ZT: High temperature regime

We did not consider the lattice phonon effects in the calculations. However, from the experimental point of view, the phononic presence could be "reduced" by employing two 1D tunneling barriers to isolate the QDs from the electrodes. The material of these devices can be appropriately chosen to produce low K_{ph} values [79]. The same effect could be obtained by the presence of an amorphous 1D conduction channel, where grain borders originate an "incoherent" contribution to the lattice thermal conductance, which act as scattering centers for phonons that contribute most strongly, reducing the thermal conductivity more than the electrical conductivity [60, 80]. However, phonons could sometimes be desirable in the DQD geometry, as in the phonon-assisted transport study in a recent paper [36]. The authors construct a DQD detuned system employing tunnel barriers and controlling the tunnel couplings to separate the electronic and thermal transport, allowing the conversion of local heat into electrical power in a nanosized heat engine.

Fig. 8 presents the δ_{eff}, ZT, S, ε, and the occupation numbers n_{QD1} and n_{QD2} vs. E_{QD1} energy. As discussed in section 2, Eq. 13 exhibits a high-temperature solution when $\delta_{eff} \simeq \pi/2$,
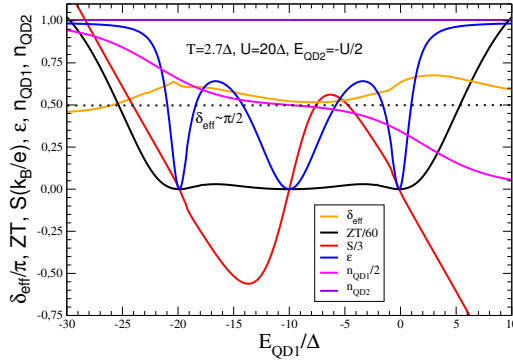
Figure 8: (Color online) Establishing the conditions to obtain an enhancement of the thermoelectric efficiency.

which is indicated by the dotted line in the figure. Furthermore, a $ZT \simeq 60$ for $E_{QD1} \simeq -30.0\Delta$ originates an $\varepsilon \simeq 1$, which implies, a high thermoelectric efficiency. The presence of the QD2 in the electron-hole symmetric condition, associated with the occupation number $n_{QD2} = 1$, and the charge fluctuations in the QD1, originates a quantum scattering process in the DQD system, analogous to the required to satisfy $\cos(2\delta) \simeq -1$ (see Fig. 2), at high temperatures, which enhances the thermoelectric efficiency.
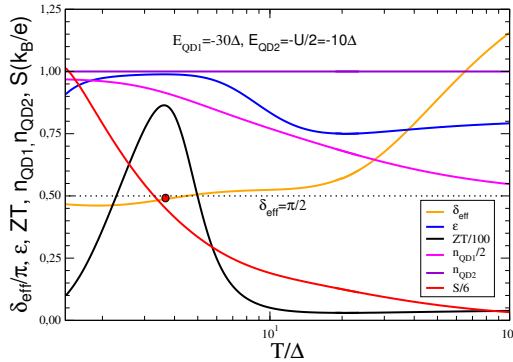
Figure 9: (Color online) The best conditions to enhance the thermoelectric efficiency considering, according to Fig. 8, $E_{QD1} = -30.0\Delta$. $S > 0$ indicates the transport by holes.

The results corresponding to $E_{QD1} = -30\Delta$ are presented in Fig. 9, with the transport ruled by holes ($S > 0$). Similarly, results with the transport ruled by electrons ($S < 0$) is presented in Fig. 10 for $E_{QD1} = 10\Delta$. In Figs. 9 and 10, the "activation" of the quantum scattering process has three common elements: the existence of electron-hole symmetry in the QD2 scattering "center", charge fluctuations in the QD1, at temperatures $T \geq \Delta$, and an effective quantum phase shift $\delta_{eff} \simeq \pi/2$.

Fig. 9 shows some properties necessary to understand the enhancement of the thermoelectric efficiency as a function of temperature: δ_{eff}, ε, ZT, n_{QD1}, n_{QD2}, and S. The charge fluctuations appear around the QD1, with its occupation number n_{QD1}, presenting a strong variation with the increase in temperature. At the same time, $QD2$ is maintained in the particle-hole symmetric situation, $n_{QD2} = 1$. This QD configuration results in the quantum scattering process that enhances the thermoelectric efficiency and is linked to charge fluctuations in the $QD1$. The highest value of $ZT \simeq 86.0$ is achieved at temperature $T = 3.66\Delta$, at around the red dot, when $\varepsilon \simeq 1$, and $\delta_{eff} \simeq \pi/2$. This setup produces an effective quantum scattering process that enhances the efficiency at finite output power, Eq. 44, $\eta_{fo} \simeq \eta_C$, close to the Carnot

efficiency η_C, for a large range of temperatures in the interval $\Delta > T > 10\Delta$. On the other hand, we do not have Kondo scattering processes in the system due to the high temperatures.

The same situation occurs in Fig. 10, for $E_{QD_1} = 10.0\Delta$, which is symmetrical to Fig. 9. The highest value of $ZT \simeq 86.0$ also occurs at temperature $T = 3.66\Delta$, with $\varepsilon \simeq 1$, and around the red dot; the δ_{eff} is close to $\pi/2$.
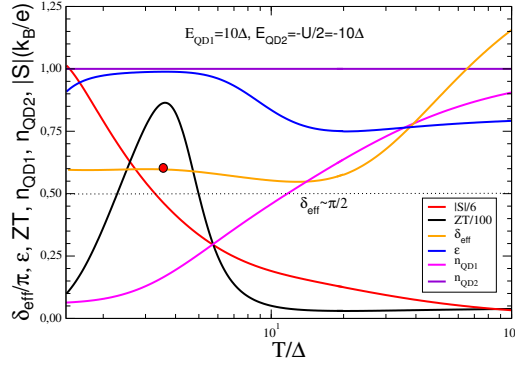
Figure 10: (Color online) The same of Fig. 9, but for $E_{QD1} = 10.0\Delta$. In this case, $S < 0$ indicates the transport by electrons.
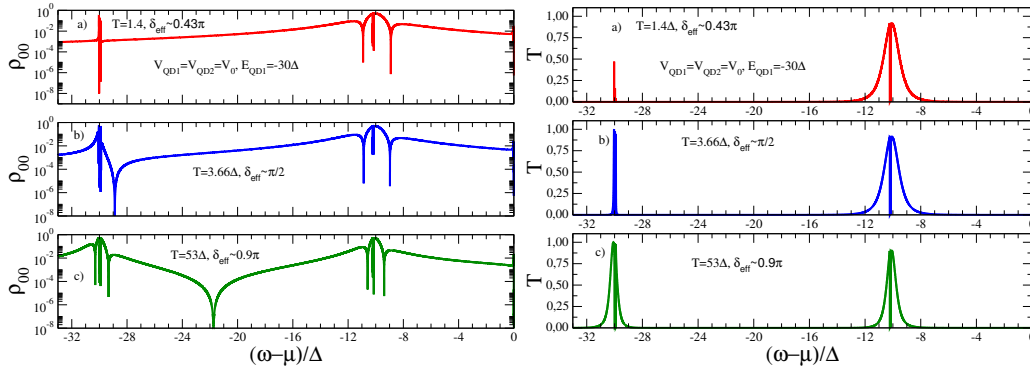
Figure 11: (Color online) Local density of states $\rho_{00}(\omega)$ and the transmittance $\mathcal{T}(\omega)$ vs. ω, for different temperatures.

In Figs. 11 (a, b, c) we plot the local density of states $\rho_{00}(\omega)$ and the transmittance $\mathcal{T}(\omega)$ vs. ω for different temperatures: a) $T = 1.4\Delta$, b) $T = 3.66\Delta$, and c) $T = 53.0\Delta$ and $E_{QD1} = -30\Delta$, $E_{QD2} = -10.0\Delta$ and $U = 20.0\Delta$. For $T = 1.4\Delta$ and $T = 3.66\Delta$, the effective quantum phase scattering is around $\delta_{eff} \simeq \pi/2$, and for $T = 53.0\Delta$, $\delta_{eff} \simeq \pi$.

The $\rho_{00}(\omega)$ exhibits two Fano-shaped structures located at $\omega - \mu = E_{QD1} = -30\Delta$ and $\omega - \mu \simeq E_{QD1} + U = -10\Delta$, that evolves with the increasing of temperature, producing a well-defined BIC at $\omega - \mu \simeq -22\Delta$ and two lateral quasi-BICs, as indicated in the $\rho_{00}(\omega)$ plot of Fig. 11c). However, as we expected, the presence of the BIC in $\rho_{00}(\omega)$ does not generate any signature in $\mathcal{T}(\omega)$. The increase of the temperature activates charge fluctuation in the QD1 from the many-body energy level $E_{QD1} + U = -10\Delta$ to the conduction channel, reducing the occupation number n_{QD1}, as indicated in Fig. 9 and, shaping the resonances at around the energies $E_{QD1} = -30\Delta$ and $E_{QD1} = -10\Delta$, as indicated in the $\mathcal{T}(\omega)$ plot of Fig. 11. Another effect observed in the plots is the spectral transfer of the states from the quasi-BIC at $\omega - \mu = \simeq -10\Delta$ to the quasi-BIC formed at $\omega - \mu \simeq -30\Delta$. We identify the rising of these structures as linked with quasi-BICs generated by thermal excitations.

Fig. 12 shows the map of the density of states of the local GF $G_{00}(\omega + i\eta)$ (Eq. 16) in the complex plane, for $E_{QD1} = -30.0\Delta$ and temperatures $T = 53.0\Delta$, $T = 3.66\Delta$ and $T = 1.4\Delta$.
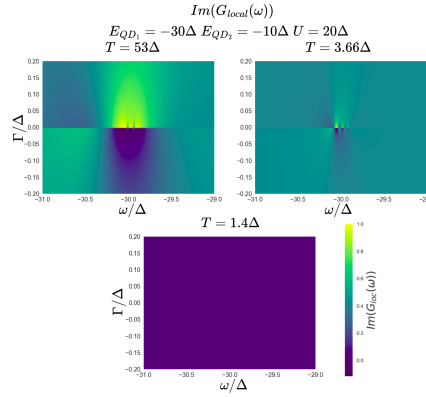
Figure 12: (Color online)Map of the density of states of the local Green function, showing the quasi-BIC formation at $E_{QD1} = -30.0\Delta$, for different temperatures.

The result presents a peak around $\omega = -30.0\Delta$ that increases its intensity as the temperature grows and is associated with the conformation of a quasi-BIC at this energy. The result is consistent with the one indicated in the $\mathcal{T}(\omega)$ plot of Fig. 11(a,b,c), where the width of the quasi-BIC peak increases with temperature.

Analogous results to those presented in Figs 11 and 12 were obtained when $E_{QD1} = 10\Delta$ at $(\omega - \mu) \simeq 10\Delta$ (not presented here). In this condition, the thermopower value changes its sign, and the results for the local density of states and the transmittance are a "mirror" with relation to the chemical potential value $(\omega - \mu) = 0.0$.

7   Conclusions and Perspectives

The study of the universal thermoelectric properties for a QD immersed in a ballistic conduction channel in the Kondo regime, described by the SIAM, permits us to obtain the "ideal" quantum phase shift associated with a quantum scattering that increases the thermoelectric efficiency of the system. We explored the possibility of enhancing the thermal efficiency of nanostructured materials, employing universal relations as a function of $T^* = \frac{T}{T_K}$. We calculated the ideal phase shifts to improve ZT at the symmetric point of the SIAM, calculating the scattering phase shift using Eq. 13, that could enhance the thermoelectric efficiency of the device, allowing the system to achieve the best dimensionless thermoelectric figure of merit ZT. However, we showed that it is not possible to achieve this condition with a single QD device in the Kondo regime immersed in a ballistic quantum wire.

To overcome this limitation, we studied a DQD system with one of the QDs "tuned" into the electron-hole symmetric condition. We showed that the DQD exhibits an "effective" quantum phase shift δ_{eff} that improves the thermoelectric efficiency of the device, allowing to achieve the best dimensionless thermoelectric figure of merit ZT, at low (Sec. 5) and high temperatures (Sec. 6).

Our results indicate that the quantum scattering-interference process, associated with enhancing the thermoelectric efficiency of the DQD system, is linked with the rise of quasi-BICs. This process happens in two situations: At low temperatures, near the chemical potential, where the competition of the charge fluctuations in the QD1 and the Kondo effect present in the QD2 originates a Fano resonance associated with a large ZT that produces a perfect conduction channel as indicated in Fig. 6. The other situation occurs at $T > \Delta$ temperature regime and generates quasi-BICs thermally activated but associated only with charge fluctu-

ations in the QD1. The QD2 continues in the particle-hole symmetric point without charge fluctuations, but the Kondo effect has disappeared due to the high-temperature regime. Those quasi-BICs are present even at high temperatures $T \simeq 50\Delta$, a point that could be important for possible system applications in thermoelectric devices. However, It is necessary to work with temperatures that do not change the symmetry electron-hole in the QD2, i.e., that do not originate charge fluctuations in the QD2. Then, a considerable U value is desirable.

The general conditions to generate BICs and quasi-Bics in the DQD setup, at low and high temperatures, have three common elements: The existence of electron-hole symmetry in one of the QDs scattering "centers" (QD2 here), an intense process of charge fluctuations in the other QD (QD1 here), and an effective quantum phase shift $\delta_{eff} \simeq 3\pi/4$ or $\pi/4$, for low temperatures and $\delta_{eff} \simeq \pi/2$ for high temperatures as derived in Fig. 2. However, there are some differences in the low and high-temperature quasi-Bics; the first is driven by the hybridization and the second by the temperature. Only one quasi-Bic exists at low temperatures, and we have twin quasi-Bic at high temperatures.

We expect that in the DQD system with localized energy values of the order of $E_{QD2} = -10.0\Delta \simeq -10^{-2}eV$, and interaction-repulsion energy $U = 2 \times |E_{QD2}| = 20.0\Delta \simeq 2 \times 10^{-2}eV$, the temperature values associated with the enhancing ZT process would be $T > \Delta \sim 10K$. The numerical results show that the maximum temperature (T_{max}), where ZT attains its maximum value is achieved approximately at $T_{max} \simeq \frac{3U}{2k_B} \times 10^{-1}$; here, k_B is the Boltzmann's constant. However, if the U parameter increases, the temperature associated with the enhancing quantum interference process of ZT also increases. In order to obtain temperatures that enhance ZT over 300K, we require $T_{max} \geq \frac{3U}{2} \times 10^{-1}\Delta \geq 300K$, $U \geq 2 \times 10^2 K \simeq 2 \times 10^{-2}eV$. We should employ systems that present strong "localization" tuned in the electron-hole symmetric point to originate a quantum scattering process that improves ZT at higher temperatures, where the Carnot's thermoelectric efficiency is high. We expect the results of this paper to motivate experimental research to submit the experimental test of our theoretical predictions.

Funding information   We are thankful for the financial support of the Research Division of the Colombia National University -Bogotá (DIEB). E. Ramos acknowledges support by Department of Science, Technology and Innovation by means of Colombian doctoral fellowship number 617-2. M. S. F. Acknowledges financial support from the Brazilian National Council for Scientific and Technological Development (CNPq) Grant. Nr. 311980/2021-0 and to Foundation for Support of Research in the State of Rio de Janeiro (FAPERJ) process Nr. 210 355/2018.

A   Cumulant Green's function method

In this appendix we present a summary of the main equations necessary to establish the Cumulant Green's Functions Method (CGFM). The exact GF for the localized electrons with spin σ can be exactly calculated though the 4×4 matrices equation (details can be found in reference [59], a brief presentation could be obtained in reference [63])

$$\mathbf{G}_\sigma(i\omega) = \mathbf{M}_\sigma(i\omega) \cdot (\mathbf{I} - \mathbf{A}_\sigma(i\omega))^{-1}, \tag{23}$$

where $i\omega$ are the Matsubara's frequencies, and from this equation follows

$$\mathbf{M}_\sigma(i\omega) = (\mathbf{I} + \mathbf{G}_\sigma(i\omega) \cdot \mathbf{W}_\sigma(i\omega))^{-1} \cdot \mathbf{G}_\sigma(i\omega), \tag{24}$$

where $\mathbf{M}_\sigma(i\omega)$ is the exact cumulant and $\mathbf{A}_\sigma(i\omega) = \mathbf{W}(i\omega) \cdot \mathbf{M}(i\omega)$. If the Hamiltonian is spin independent or commutes with the z component of the spin, all matrices can be reduced to

two 2×2 matrices, being that $\mathbf{W}(z)$ matrix is defined by

$$\mathbf{W}_\uparrow(z) = |V|^2 \, \varphi_\uparrow(z) \begin{pmatrix} 1 & 1 \\ 1 & 1 \end{pmatrix}, \tag{25}$$

$$\mathbf{W}_\downarrow(z) = |V|^2 \, \varphi_\downarrow(z) \begin{pmatrix} 1 & -1 \\ -1 & 1 \end{pmatrix}. \tag{26}$$

where $z = \omega + i\eta$ corresponds to the analytic continuation of the Matsubara frequencies to the real axis, with $\eta = 0.0001$ is a small real quantity employed in the numerical calculations. Considering a rectangular band with half-width D we can write

$$\varphi_\sigma(z) = \frac{1}{2D} \, \ln\left(\frac{z - D + \mu}{z + D + \mu}\right). \tag{27}$$

The calculation of the exact cumulants correspond to the exact solution of the Hamiltonian, what is out of question here. Therefore, we introduce an approximation that consists in substituting the exact solution for an atomic cumulant that is defined by the atomic GF, that are calculated employing the Lehmann spectral representation

$$\mathcal{G}^{at}_{\alpha\alpha'}(i\omega_s) = -e^{\beta\Omega} \sum_{n,r,r'} \frac{\exp(-\beta\varepsilon_{n-1,r}) + \exp(-\beta\varepsilon_{n,r'})}{i\omega_s + \varepsilon_{n-1,r} - \varepsilon_{n,r'}} \times$$

$$\times \langle n-1, r | \, X_{j,\alpha} \, | n, r' \rangle \langle n, r' | \, X^\dagger_{j,\alpha'} \, | n-1, r \rangle, \tag{28}$$

where Ω is the Thermodynamical potential and $\epsilon = E_d - \mu$ corresponds to the eigenvalue minus the chemical potential. This equation can be rewritten as

$$G^{at}_\sigma(z) = e^{\beta\Omega} \sum_{i=1}^{M} \frac{m_{i\sigma}}{z - u_{i\sigma}}, \tag{29}$$

where the $u_{i\sigma}$ and $m_{i\sigma}$ are the poles and the residues of the atomic GF of the localized electrons respectively.

The atomic solution of the exact Green's functions $\mathbf{G}_\sigma(z)$ follows the same rule as the equation 23. Therefore, the atomic cumulants follows the equation

$$\mathbf{M}^{at}_\sigma(z) = \left(\mathbf{I} + \mathbf{G}^{at}_\sigma(\mathbf{z}) \cdot \mathbf{W}^o_\sigma(z)\right)^{-1} \cdot \mathbf{G}^{at}_\sigma(z), \tag{30}$$

where the $\mathbf{W}^o_\sigma(z)$ is equal to

$$\mathbf{W}^o_\uparrow(z) = |\Delta|^2 \, \varphi^o_\uparrow(z) \begin{pmatrix} 1 & 1 \\ 1 & 1 \end{pmatrix}, \tag{31}$$

$$\mathbf{W}^o_\downarrow(z) = |\Delta|^2 \, \varphi^o_\downarrow(z) \begin{pmatrix} 1 & -1 \\ -1 & 1 \end{pmatrix}, \tag{32}$$

where $\Delta = \pi V^2/2D$ is the Anderson parameter that replace the hybridization in the atomic case. This normalization is needed because the use of the true hybridization V superestimate the contribution of the conduction electrons, once we concentrate them in a single energy level ϵ_0 where

$$\varphi^o_\sigma(z) = \frac{-1}{z - \varepsilon_o - \mu}, \tag{33}$$

is the GF of the zero-width band. The CGFM consists in substituting the atomic cumulant $\mathbf{M}^{at}_\sigma(z)$ in the exact equation for the full Green function, Eq. 23. Details and the final expressions for all the GFs can be found in the reference [59].

B Thermoelectric transport properties

Following a standard procedure [81–83], we calculated the thermoelectric transport properties through a quantum dot in the steady-state condition immersed in the right (cold) and left (left) leads as indicated in Fig. 1. We considered the system under an applied a small external bias voltage $\Delta V = V_L - V_R$ and a small temperature difference $\Delta T = T_L - T_R$. We also considered the chemical potential fixed at ($\mu = 0$). The charge current J_e and the heat current J_Q are given by:

$$J_e = e^2 L_0(T)(-\Delta V) + \frac{e}{T} L_1(T)(-\Delta T), \tag{34}$$

$$J_Q = e L_1(T)(-\Delta V) + \frac{1}{T} L_2(T)(-\Delta T), \tag{35}$$

where e denotes the magnitude of the electrical charge and $L_0(T)$, $L_1(T)$, and $L_2(T)$ are the transport coefficients.

The electron conductance G is measured under isothermal conditions $\Delta T = 0$. From Eq. (34) we get

$$J_e = e^2 L_0(T)(-\Delta V), \tag{36}$$

and from the definition of electrical conductance [83, 84]

$$G(T) = -\lim_{\Delta V \to 0} \frac{J_e}{\Delta V}\bigg|_{\Delta T = 0} = e^2 L_0(T). \tag{37}$$

The electronic contribution to the thermal conductance κ is usually measured by putting the sample on an open electrical circuit in such a way that $J_e = 0$ [82]. From Eq. (34)

$$(-\Delta V) = \frac{1}{eT} \frac{L_1(T)}{L_0(T)} (\Delta T). \tag{38}$$

Substituting Eq. (38) into Eq. (35) we get

$$J_Q = \frac{1}{T}\left(L_2(T) - \frac{L_1^2(T)}{L_0(T)}\right)(-\Delta T), \tag{39}$$

and from the definition of the thermal conductance [83, 84]

$$\kappa(T) = -\lim_{\Delta T \to 0} \frac{J_Q}{\Delta T}\bigg|_{J_e = 0} = \frac{1}{T}\left(L_2(T) - \frac{L_1^2(T)}{L_0(T)}\right). \tag{40}$$

The thermopower (Seebeck effect) is defined by the relation [83, 84]

$$S(T) = \lim_{\Delta T \to 0} \frac{\Delta V}{\Delta T}\bigg|_{J_e = 0} = \left(\frac{-1}{eT}\right)\frac{L_1(T)}{L_0(T)}. \tag{41}$$

The Boltzmann equation is only valid in the semiclassical regime, where the electrons behave as well-defined wave packets. Generally, this condition is satisfied at sufficiently high temperatures where the electron coherence is destroyed due to the strong inelastic scattering (diffusive transport). In this limit, the mean free path (l) is much larger than the electronic wavelength λ, ($l >> \lambda$). However, at low temperatures in the full quantum regime ($l << \lambda$), the electrons behave as waves (ballistic transport), the electron coherence is strong, and new phenomena arise that only a full quantum mechanics formalism can take into account (Landauer formalism for example), and the Boltzmann equation is not valid anymore. A comparison between the applicability limits of both methods can be found in the reference [85].

As examples of new full quantum phenomena [86], we have the Anderson localization, electronic transport in topological materials, far-from-equilibrium phenomena such as shot noise, and bound states in the continuum (BICs) as studied in this paper.

We calculate the linear transport coefficients $L_0(T)$, $L_1(T)$, and $L_2(T)$, following the reference [62]. The transport coefficients are consistent with the general thermoelectric formulas derived earlier and are given by

$$L_n(T) = \frac{2}{h} \int \left(-\frac{\partial f(\epsilon, T)}{\partial \epsilon} \right) \epsilon^n \mathcal{T}(\epsilon, T) d\epsilon, \tag{42}$$

where $\mathcal{T}(\omega, T)$ is the transmittance for the electrons with energy $\epsilon = \hbar\omega$ and temperature T, here h is the reduced Planck's constant and $f(\omega, T)$ is the Fermi-Dirac distribution function [83, 84].

On general grounds, we followed Mahan and Sofo's paper associating the efficiency to the ZT parameter. However, we include a more detailed analysis of the efficiency at maximal output power (mo), η_{mo}, and at finite output power (fo) η_{fo}.

It is well known that Carnot's efficiency η_C bounds the efficiency of all kinds of heat engines and is associated with a reversible engine with a zero production of entropy $\Delta S = 0$ and an infinity time for the working cycle to be completed. However, in "real" irreversible systems $\Delta S > 0$, the working cycle time is always finite. The study of η_{mo} efficiency in "real" irreversible systems has attracted much attention [87–89]. Curzon and Ahlborn [88] derived an upper bound limit, η_{mo} efficiency, from an endoreversible Carnot heat engine: $\eta_{mo} = 1 - \sqrt{1 - \eta_C}$. On the other hand, the lower bound limit of the η_{mo} efficiency that is relevant for the present work was obtained for fermionic thermochemical engines [89], with an infinitesimal width for the transmission coefficient $\Gamma \to 0$, and is given by [90]

$$\eta_{mo} \geq \eta_C / (1 + a(2 - \eta_C)), \tag{43}$$

with $a = 0.93593$. The η_{fo} is given by

$$\eta_{fo} = \eta_C (\sqrt{ZT + 1} - 1)/(\sqrt{ZT + 1} + 1). \tag{44}$$

Recently, it was obtained experimentally a $\eta_{mo} \simeq 0.7\eta_C$, consistent with symmetric dissipation, in a QD system of InAs/InP [64].

References

[1] A. F. Iofee, *Semiconductor Thermoelements and Thermoelectric Cooling*, Infosearch, London, 1 edn. (1957).

[2] D. A. Wright, *Thermoelectric properties of bismuth telluride and its alloys*, Nature **181**(4612), 834 (1958), doi:10.1038/181834a0.

[3] A. F. Joffe and L. S. Stil, *Physical problems of thermoelectricity*, Reports on Progress in Physics **22**, 167 (1959).

[4] P. Alexandre, S. Susanna and S. Lírio, *History of development of thermoelectric materials for electric power generation and criteria of their quality*, Materials Research **17**, 1260 (2014), doi:10.1590/1516-1439.272214.

[5] I. T. Witting, T. C. Chasapis, F. Ricci, M. Peters, N. A. Heinz, G. Hautier and G. J. Snyder, *The thermoelectric properties of bismuth telluride*, Advanced Electronic Materials **5**(6), 1800904 (2019).

[6] P. Fernández-Yanez, V. Romero, O. Armas and G. Cerretti, *Thermal management of thermoelectric generators for waste energy recovery*, Applied Thermal Engineering **196**, 117291 (2021), doi:https://doi.org/10.1016/j.applthermaleng.2021.117291.

[7] D. Goldhaber-Gordon, J. Gores, H. Shtrikman, D. Mahalu, U. Meirav and M. Kastner, *The kondo effect in a single-electron transistor*, Materials Science and Engineering: B **84**(1), 17 (2001), doi:https://doi.org/10.1016/S0921-5107(01)00550-5.

[8] R. Scheibner, H. Buhmann, D. Reuter, M. N. Kiselev and L. W. Molenkamp, *Thermopower of a kondo spin-correlated quantum dot*, Phys. Rev. Lett. **95**, 176602 (2005), doi:10.1103/PhysRevLett.95.176602.

[9] R. Scheibner, E. G. Novik, T. Borzenko, M. König, D. Reuter, A. D. Wieck, H. Buhmann and L. W. Molenkamp, *Sequential and cotunneling behavior in the temperature-dependent thermopower of few-electron quantum dots*, Phys. Rev. B **75**, 041301 (2007), doi:10.1103/PhysRevB.75.041301.

[10] R. Scheibner, M. König, D. Reuter, A. D. Wieck, C. Gould, H. Buhmann and L. W. Molenkamp, *Quantum dot as thermal rectifier*, New Journal of Physics **10**(8), 083016 (2008), doi:10.1088/1367-2630/10/8/083016.

[11] A. Svilans, M. Josefsson, A. M. Burke, S. Fahlvik, C. Thelander, H. Linke and M. Leijnse, *Thermoelectric characterization of the kondo resonance in nanowire quantum dots*, Phys. Rev. Lett. **121**, 206801 (2018), doi:10.1103/PhysRevLett.121.206801.

[12] M. A. Manya, G. B. Martins and M. S. Figueira, *Spin-orbit coupling effects on thermoelectric transport properties in quantum dots*, Phys. Rev. B **105**, 165421 (2022), doi:10.1103/PhysRevB.105.165421.

[13] D. Prete, P. A. Erdman, V. Demontis, V. Zannier, D. Ercolani, L. Sorba, F. Beltram, F. Rossella, F. Taddei and S. Roddaro, *Thermoelectric conversion at 30 k in inas/inp nanowire quantum dots*, Nano Letters **19**(5), 3033 (2019), doi:10.1021/acs.nanolett.9b00276.

[14] A. C. Seridonio, M. Yoshida and L. N. Oliveira, *Thermal dependence of the zero-bias conductance through a nanostructure*, EPL (Europhysics Letters) **86**(6), 67006 (2009), doi:10.1209/0295-5075/86/67006.

[15] M. Yoshida, A. C. Seridonio and L. N. Oliveira, *Universal zero-bias conductance for the single-electron transistor*, Phys. Rev. B **80**, 235317 (2009), doi:10.1103/PhysRevB.80.235317.

[16] A. C. Seridonio, M. Yoshida and L. N. Oliveira, *Universal zero-bias conductance through a quantum wire side-coupled to a quantum dot*, Phys. Rev. B **80**, 235318 (2009), doi:10.1103/PhysRevB.80.235318.

[17] L. N. Oliveira, M. Yoshida and A. C. Seridonio, *Universal conductance for the anderson model*, Journal of Physics: Conference Series **200**(5), 052020 (2010), doi:10.1088/1742-6596/200/5/052020.

[18] M. Yoshida and L. Oliveira, *Thermoelectric effects in quantum dots*, Physica B: Condensed Matter **404**(19), 3312 (2009), doi:https://doi.org/10.1016/j.physb.2009.07.118.

[19] T. A. Costi and V. Zlatic, *Thermoelectric transport through strongly correlated quantum dots*, Phys. Rev. B **81**, 235127 (2010), doi:10.1103/PhysRevB.81.235127.

[20] S. Hershfield, K. A. Muttalib and B. J. Nartowt, *Nonlinear thermoelectric transport: A class of nanodevices for high efficiency and large power output*, Phys. Rev. B **88**, 085426 (2013), doi:10.1103/PhysRevB.88.085426.

[21] S. Donsa, S. Andergassen and K. Held, *Double quantum dot as a minimal thermoelectric generator*, Phys. Rev. B **89**, 125103 (2014), doi:10.1103/PhysRevB.89.125103.

[22] V. Talbo, J. Saint-Martin, S. Retailleau and P. Dollfus, *Non-linear effects and thermoelectric efficiency of quantum dot-based single-electron transistors*, Scientific Reports **7**(1), 14783 (2017), doi:10.1038/s41598-017-14009-4.

[23] T. A. Costi, *Magnetic field dependence of the thermopower of kondo-correlated quantum dots*, Phys. Rev. B **100**, 161106 (2019), doi:10.1103/PhysRevB.100.161106.

[24] T. A. Costi, *Magnetic field dependence of the thermopower of kondo-correlated quantum dots: Comparison with experiment*, Phys. Rev. B **100**, 155126 (2019), doi:10.1103/PhysRevB.100.155126.

[25] Y. Kleeorin, H. Thierschmann, H. Buhmann, A. Georges, L. W. Molenkamp and Y. Meir, *How to measure the entropy of a mesoscopic system via thermoelectric transport*, Nature Communications **10**(1), 5801 (2019).

[26] U. Eckern and K. I. Wysokiński, *Two- and three-terminal far-from-equilibrium thermoelectric nano-devices in the kondo regime*, New Journal of Physics **22**(1), 013045 (2020), doi:10.1088/1367-2630/ab6874.

[27] J. P. Heremans, C. M. Thrush and D. T. Morelli, *Thermopower enhancement in lead telluride nanostructures*, Phys. Rev. B **70**, 115334 (2004), doi:10.1103/PhysRevB.70.115334.

[28] E. A. Hoffmann, H. A. Nilsson, J. E. Matthews, N. Nakpathomkun, A. I. Persson, L. Samuelson and H. Linke, *Measuring temperature gradients over nanometer length scales*, Nano Letters **9**(2), 779 (2009).

[29] B. Dutta, J. T. Peltonen, D. S. Antonenko, M. Meschke, M. A. Skvortsov, B. Kubala, J. König, C. B. Winkelmann, H. Courtois and J. P. Pekola, *Thermal conductance of a single-electron transistor*, Phys. Rev. Lett. **119**, 077701 (2017), doi:10.1103/PhysRevLett.119.077701.

[30] N. Hartman, C. Olsen, S. Lüscher, M. Samani, S. Fallahi, G. C. Gardner, M. Manfra and J. Folk, *Direct entropy measurement in a mesoscopic quantum system*, Nature Physics **14**(11), 1083 (2018), doi:10.1038/s41567-018-0250-5.

[31] B. Dutta, D. Majidi, A. García Corral, P. A. Erdman, S. Florens, T. A. Costi, H. Courtois and C. B. Winkelmann, *Direct probe of the seebeck coefficient in a kondo-correlated single-quantum-dot transistor*, Nano Letters **19**(1), 506 (2019), doi:10.1021/acs.nanolett.8b04398.

[32] J. He and T. M. Tritt, *Advances in thermoelectric materials research: Looking back and moving forward*, Science **357**(6358) (2017).

[33] D. Sánchez and R. López, *Nonlinear phenomena in quantum thermoelectrics and heat*, Comptes Rendus Physique **17**(10), 1060 (2016).

[34] G. Benenti, G. Casati, K. Saito and R. S. Whitney, *Fundamental aspects of steady-state conversion of heat to work at the nanoscale*, Physics Reports **694**, 1 (2017).

[35] A. Hofmann, C. Karlewski, A. Heimes, C. Reichl, W. Wegscheider, G. Schön, K. Ensslin, T. Ihn and V. F. Maisi, *Phonon spectral density in a gaas/algaas double quantum dot*, Phys. Rev. Res. **2**, 033230 (2020), doi:10.1103/PhysRevResearch.2.033230.

[36] S. Dorsch, A. Svilans, M. Josefsson, B. Goldozian, M. Kumar, C. Thelander, A. Wacker and A. Burke, *Heat driven transport in serial double quantum dot devices*, Nano Letters **21**(2), 988 (2021), doi:10.1021/acs.nanolett.0c04017.

[37] C. W. Hsu, B. Zhen, A. D. Stone, J. D. Joannopoulos and M. Soljačić, *Bound states in the continuum*, Nature Reviews Materials **1**(9), 16048 (2016), doi:10.1038/natrevmats.2016.48.

[38] J. von Neuman and E. Wigner, *Uber merkwürdige diskrete Eigenwerte. Uber das Verhalten von Eigenwerten bei adiabatischen Prozessen*, Physikalische Zeitschrift **30**, 467 (1929).

[39] M. L. L. d. Guevara, F. Claro and P. A. Orellana, *Ghost fano resonance in a double quantum dot molecule attached to leads*, Phys. Rev. B **67**, 195335 (2003), doi:10.1103/PhysRevB.67.195335.

[40] M. L. Ladrón de Guevara and P. A. Orellana, *Electronic transport through a parallel-coupled triple quantum dot molecule: Fano resonances and bound states in the continuum*, Phys. Rev. B **73**, 205303 (2006), doi:10.1103/PhysRevB.73.205303.

[41] C. S. Kim, A. M. Satanin, Y. S. Joe and R. M. Cosby, *Resonant tunneling in a quantum waveguide: Effect of a finite-size attractive impurity*, Phys. Rev. B **60**, 10962 (1999), doi:10.1103/PhysRevB.60.10962.

[42] A. F. Sadreev, *Interference traps waves in an open system: bound states in the continuum*, Reports on Progress in Physics **84**(5), 055901 (2021), doi:10.1088/1361-6633/abefb9.

[43] U. Fano, *Effects of configuration interaction on intensities and phase shifts*, Phys. Rev. **124**, 1866 (1961), doi:10.1103/PhysRev.124.1866.

[44] E. Melik-Gaykazyan, K. Koshelev, J.-H. Choi, S. S. Kruk, A. Bogdanov, H.-G. Park and Y. Kivshar, *From fano to quasi-bic resonances in individual dielectric nanoantennas*, Nano Letters **21**(4), 1765 (2021), doi:10.1021/acs.nanolett.0c04660.

[45] M. Amrani, S. Khattou, H. Al-Wahsh, Y. Rezzouk, E. H. E. Boudouti, C. Ghouila-Houri, A. Talbi, A. Akjouj, L. Dobrzynski and B. Djafari-Rouhani, *Bound states in the continuum and fano resonances in photonic and plasmonic loop structures*, Optical and Quantum Electronics **54**(9), 599 (2022), doi:10.1007/s11082-022-03991-3.

[46] P. Trocha and J. Barnaś, *Large enhancement of thermoelectric effects in a double quantum dot system due to interference and coulomb correlation phenomena*, Phys. Rev. B **85**, 085408 (2012), doi:10.1103/PhysRevB.85.085408.

[47] García-Suárez, V. M., R. Ferradás and J. Ferrer, *Impact of fano and breit-wigner resonances in the thermoelectric properties of nanoscale junctions*, Phys. Rev. B **88**, 235417 (2013), doi:10.1103/PhysRevB.88.235417.

[48] R.-N. Wang, G.-Y. Dong, S.-F. Wang, G.-S. Fu and J.-L. Wang, *Impact of contact couplings on thermoelectric properties of anti, fano, and breit-wigner resonant junctions*, Journal of Applied Physics **120**(18), 184303 (2016), doi:10.1063/1.4967751.

[49] J. A. Briones-Torres, R. Pérez-Álvarez, S. Molina-Valdovinos and I. Rodríguez-Vargas, *Enhancement of the thermoelectric properties in bilayer graphene structures induced by fano resonances*, Scientific Reports **11**(1), 13872 (2021), doi:10.1038/s41598-021-93220-w.

[50] G. D. Mahan and J. O. Sofo, *The best thermoelectric*, Proceedings of the National Academy of Sciences **93**(15), 7436 (1996), doi:10.1073/pnas.93.15.7436.

[51] C. Jeong, R. Kim and M. S. Lundstrom, *On the best bandstructure for thermoelectric performance: A Landauer perspective*, Journal of Applied Physics **111**(11), 113707 (2012), doi:10.1063/1.4727855.

[52] R. Ferradás, V. M. García-Suárez and J. Ferrer, *Symmetry-induced quantum interference effects in metalloporphyrin wires*, Journal of Physics: Condensed Matter **25**(32), 325501 (2013), doi:10.1088/0953-8984/25/32/325501.

[53] Z.-F. Liu, S. Wei, H. Yoon, O. Adak, I. Ponce, Y. Jiang, W.-D. Jang, L. M. Campos, L. Venkataraman and J. B. Neaton, *Control of single-molecule junction conductance of porphyrins via a transition-metal center*, Nano Letters **14**(9), 5365 (2014), doi:10.1021/nl5025062.

[54] Q. H. Al-Galiby, H. Sadeghi, L. A. Algharagholy, I. Grace and C. Lambert, *Tuning the thermoelectric properties of metallo-porphyrins*, Nanoscale **8**, 2428 (2016), doi:10.1039/C5NR06966A.

[55] M. Noori, A. C. Aragones, G. Di Palma, N. Darwish, S. W. D. Bailey, Q. Al-Galiby, I. Grace, D. B. Amabilino, A. González-Campo, I. Díez-Pérez and C. J. Lambert, *Tuning the electrical conductance of metalloporphyrin supramolecular wires*, Scientific Reports **6**(1), 37352 (2016), doi:10.1038/srep37352.

[56] D. F. Aranguren-Quintero, E. Ramos, J. Silva-Valencia, M. S. Figueira, L. N. Oliveira and R. Franco, *Universality and thermoelectric transport properties of quantum dot systems*, Phys. Rev. B **103**, 085112 (2021), doi:10.1103/PhysRevB.103.085112.

[57] M. Grobis, I. G. Rau, R. M. Potok, H. Shtrikman and D. Goldhaber-Gordon, *Universal scaling in nonequilibrium transport through a single channel kondo dot*, Phys. Rev. Lett. **100**, 246601 (2008), doi:10.1103/PhysRevLett.100.246601.

[58] J. J. Parks, A. R. Champagne, T. A. Costi, W. W. Shum, A. N. Pasupathy, E. Neuscamman, S. Flores-Torres, P. S. Cornaglia, A. A. Aligia, C. A. Balseiro, G. K.-L. Chan, H. D. Abruña *et al.*, *Mechanical control of spin states in spin-1 molecules and the underscreened kondo effect*, Science **328**(5984), 1370 (2010), doi:10.1126/science.1186874.

[59] T. Lobo, M. S. Figueira and M. E. Foglio, *The atomic approach to the anderson model for the finite u case: application to a quantum dot*, Nanotechnology **21**, 274007 (2010), doi:10.1088/0957-4484/21/27/274007.

[60] C. J. Vineis, A. Shakouri, A. Majumdar and M. G. Kanatzidis, *Nanostructured thermoelectrics: Big efficiency gains from small features*, Adv. Mater. **22**(36), 3970 (2010), doi:10.1002/adma.201000839.

[61] B. Ryu, J. Chung, M. Kumagai, T. Mato, Y. Ando, S. Gunji, A. Tanaka, D. Yana, M. Fujimoto, Y. Imai, Y. Katsura and S. Park, *Best thermoelectric efficiency of ever-explored materials*, iScience **26**(4), 106494 (2023), doi:https://doi.org/10.1016/j.isci.2023.106494.

[62] B. Dong and X. L. Lei, *Effect of the kondo correlation on the thermopower in a quantum dot*, Journal of Physics: Condensed Matter **14**(45), 11747 (2002), doi:10.1088/0953-8984/14/45/316.

[63] E. Ramos, J. Silva-Valencia, R. Franco and M. S. Figueira, *The thermoelectric figure of merit for the single electron transistor*, International Journal of Thermal Sciences **86**, 387 (2014), doi:https://doi.org/10.1016/j.ijthermalsci.2014.07.018.

[64] M. Josefsson, A. Svilans, A. M. Burke, E. A. Hoffmann, S. Fahlvik, C. Thelander, M. Leijnse and H. Linke, *A quantum-dot heat engine operating close to the thermodynamic efficiency limits*, Nature Nanotechnology **13**(10), 920 (2018), doi:10.1038/s41565-018-0200-5.

[65] D. Pérez Daroca, P. Roura-Bas and A. A. Aligia, *Enhancing the nonlinear thermoelectric response of a correlated quantum dot in the kondo regime by asymmetrical coupling to the leads*, Phys. Rev. B **97**, 165433 (2018), doi:10.1103/PhysRevB.97.165433.

[66] G. Gomez-Silva, P. A. Orellana and E. V. Anda, *Enhancement of the thermoelectric efficiency in a t-shaped quantum dot system in the linear and nonlinear regimes*, Journal of Applied Physics **123**(8), 085706 (2018), doi:10.1063/1.5019922.

[67] A. Manaparambil and I. Weymann, *Nonequilibrium seebeck effect and thermoelectric efficiency of kondo-correlated molecular junctions*, Phys. Rev. B **107**, 085404 (2023), doi:10.1103/PhysRevB.107.085404.

[68] K. Kang, S. Y. Cho, J.-J. Kim and S.-C. Shin, *Anti-kondo resonance in transport through a quantum wire with a side-coupled quantum dot*, Phys. Rev. B **63**, 113304 (2001), doi:10.1103/PhysRevB.63.113304.

[69] G. Ordonez, K. Na and S. Kim, *Bound states in the continuum in quantum-dot pairs*, Phys. Rev. A **73**, 022113 (2006), doi:10.1103/PhysRevA.73.022113.

[70] L. H. Guessi, F. A. Dessotti, Y. Marques, L. S. Ricco, G. M. Pereira, P. Menegasso, M. de Souza and A. C. Seridonio, *Encrypting majorana fermion qubits as bound states in the continuum*, Phys. Rev. B **96**, 041114 (2017), doi:10.1103/PhysRevB.96.041114.

[71] Y. Kruglyak, *Landauer-datta-lundstrom generalized transport model for nanoelectronics*, Journal of Nanoscience **2014**, 725420 (2014), doi:10.1155/2014/725420.

[72] T. Taniguchi and M. Büttiker, *Friedel phases and phases of transmission amplitudes in quantum scattering systems*, Phys. Rev. B **60**, 13814 (1999), doi:10.1103/PhysRevB.60.13814.

[73] A. Levy Yeyati and M. Büttiker, *Scattering phases in quantum dots: An analysis based on lattice models*, Phys. Rev. B **62**, 7307 (2000), doi:10.1103/PhysRevB.62.7307.

[74] B. Solís, M. Ladrón de Guevara and P. Orellana, *Friedel phase discontinuity and bound states in the continuum in quantum dot systems*, Physics Letters A **372**(26), 4736 (2008), doi:https://doi.org/10.1016/j.physleta.2008.05.014.

[75] G. Rajput, P. K. Ahluwalia and K. C. Sharma, *Partial swapping of fano resonance and bound states in continuum in a correlated double-quantum-dot system*, EPL (Europhysics Letters) **94**(1), 17003 (2011), doi:10.1209/0295-5075/94/17003.

[76] W. G. van der Wiel, S. D. Franceschi, T. Fujisawa, J. M. Elzerman, S. Tarucha and L. P. Kouwenhoven, *The kondo effect in the unitary limit*, Science **289**(5487), 2105 (2000), doi:10.1126/science.289.5487.2105.

[77] A. V. Kretinin, H. Shtrikman, D. Goldhaber-Gordon, M. Hanl, A. Weichselbaum, J. von Delft, T. Costi and D. Mahalu, *Spin-$\frac{1}{2}$ kondo effect in an inas nanowire quantum dot: Unitary limit, conductance scaling, and zeeman splitting*, Phys. Rev. B **84**, 245316 (2011), doi:10.1103/PhysRevB.84.245316.

[78] I. Rotter and A. F. Sadreev, *Zeros in single-channel transmission through double quantum dots*, Phys. Rev. E **71**, 046204 (2005), doi:10.1103/PhysRevE.71.046204.

[79] X. Zianni, *Thermoelectric metamaterials: Nano-waveguides for thermoelectric energy conversion and heat management at the nanoscale*, Advanced Electronic Materials **7**(8), 2100176 (2021), doi:https://doi.org/10.1002/aelm.202100176.

[80] M. Dresselhaus, G. Chen, M. Tang, R. Yang, H. Lee, D. Wang, Z. Ren, J.-P. Fleurial and P. Gogna, *New directions for low-dimensional thermoelectric materials*, Advanced Materials **19**(8), 1043 (2007), doi:https://doi.org/10.1002/adma.200600527.

[81] G. D. Mahan, *Many-particle physics*, Many-Particle Physics - Springer p. 227 (1990).

[82] J. M. Ziman, *Principles of the theory of solids*, Principles of the Theory of Solids - Cambridge University Press pp. 229–239 (1999).

[83] T. A. Costi and V. Zlatić, *Thermoelectric transport through strongly correlated quantum dots*, Phys. Rev. B **81**, 235127 (2010), doi:10.1103/PhysRevB.81.235127.

[84] M.Yoshida and L.N.Oliveira, *Thermoelectric effects in quantum dots*, Physica B: Condensed Matter **404**, 3312 (2009), doi:10.1016/j.physb.2009.07.118.

[85] C. Jeong, R. Kim, M. Luisier, S. Datta and M. Lundstrom, *On Landauer versus Boltzmann and full band versus effective mass evaluation of thermoelectric transport coefficients*, Journal of Applied Physics **107**(2), 023707 (2010), doi:10.1063/1.3291120.

[86] K. Kawabata and M. Ueda, *Nonlinear landauer formula: Nonlinear response theory of disordered and topological materials*, Phys. Rev. B **106**, 205104 (2022), doi:10.1103/PhysRevB.106.205104.

[87] M. Esposito, R. Kawai, K. Lindenberg and C. Van den Broeck, *Efficiency at maximum power of low-dissipation carnot engines*, Phys. Rev. Lett. **105**, 150603 (2010), doi:10.1103/PhysRevLett.105.150603.

[88] F. L. Curzon and B. Ahlborn, *Efficiency of a Carnot engine at maximum power output*, American Journal of Physics **43**(1), 22 (1975), doi:10.1119/1.10023.

[89] X. Luo, N. Liu and T. Qiu, *Efficiency at maximum power of thermochemical engines with near-independent particles*, Phys. Rev. E **93**, 032125 (2016), doi:10.1103/PhysRevE.93.032125.

[90] H. S. Kim, W. Liu, G. Chen, C.-W. Chu and Z. Ren, *Relationship between thermoelectric figure of merit and energy conversion efficiency*, Proceedings of the National Academy of Sciences **112**, 8205 (2015), doi:10.1073/pnas.1510231112.